Substrate Effects in Hysteresis of Microscale Ni-Mn-Sn Heusler Alloy Films

Yijia Zhang[1]
Dexin Zhao[1]
Carlos Lago[1]
Kelvin Xie[1]
Patrick J. Shamberger[1, *]

[1] Department of Materials Science and Engineering
Texas A&M University
College Station, TX, 77843, USA

Phone: 979-458-1086
Fax: 979-862-6835
E-mail: patrick.shamberger@tamu.edu

Abstract

During martensitic phase transformations in thin films, substrates impact hysteresis by introducing an additional interface, which can inhibit martensite/austenite interface motion. In order to reduce hysteresis, we examine 2.9-14.5 μm thick Ni-Mn-Sn films which in some cases have been delaminated from the substrates before or after annealing. We compare thermal hysteresis and defect densities at the interface. Delaminating films prior to annealing decreases hysteresis, whereas delaminating films after annealing does not significantly impact hysteresis. Substrate effects are attributed to the thermal expansion mismatch between the film and substrate, resulting in dislocations at the interface and consequentially, an increase in hysteresis.

Keywords: Martensitic phase transformation; thin films; Heusler phases; internal friction.

Manuscript

Caloric effect materials based on reversible first-order phase transformations have the potential to enable high efficiency refrigeration technologies [1-3]. Microscale and nanoscale multifunctional films and wires with large surface to volume ratios are of interest due to their rapid heat transfer into a surrounding heat transfer fluid, thereby increasing cycle frequencies and average cooling powers [4]. However, different parameters, including size and shape of materials and stress-coupling, might impact the thermal hysteresis significantly [5-9]. As an example, when the thickness of epitaxial Ni-Mn-Ga films is reduced to 40 nm, martensitic phase transformations during cooling are inhibited [10], while the inhibited martensitic phase transformation is allowed after removing the sacrificial substrate by etching [11]. A common characteristic of these films and wires, whose thermal hysteresis tends to increase as the critical length scale decreases, is the formation of the alloy/substrate interface during fabrication. Therefore, improving the understanding of the role of the substrate on the general nature of the martensitic phase transformations is necessary in order to decrease their hysteresis and maximize the efficiency of a cooling cycle.

A number of physical mechanisms may contribute to hysteresis during martensitic phase transformations in thin multifunctional alloy films, including 1) nucleation energy barrier which must be overcome to initiate transformations [12-14], 2) lattice mismatch resulting in film strain which delayed the transformations in thin epitaxial films [10,15,16], and 3) internal frictional work which is associated with frictional barriers of martensite/austenite interface motion [5,10]. It has been suggested that thermal expansion mismatch at the film/substrate interface during the cooling process of heat treatment results in residual strain, which generates defects and internal friction near the interface during martensitic transformations [5,17]. Doyle et al. have reported that the values of residual stresses in 0.1 to 5 μm thick Ni-Mn-Ga films depended on different substrates and film thickness [18]. Here, we investigate the role of the alloy/substrate interface on the hysteresis of martensitic transformations in 1) Ni-Mn-Sn alloy films on substrates 2) free-standing alloy grains whose substrates are removed after annealing, and 3) free-standing alloy films whose substrates are removed before annealing. We find that removing substrates before annealing decreases the hysteresis (25 %, 27 %, and 34 % decrease in 14.5, 8.7, and 2.9 μm thick films, respectively), while removing substrates after annealing does not significantly impact hysteresis. Compared with the free-standing film, the dislocation density was increased at the film/substrate interface of film on substrate. Thus, we infer that thickness-dependent hysteresis in microscale alloy films on substrates is partially attributed to the thermal expansion mismatch at the film/substrate interfaces during the annealing step.

$Ni_{0.48}Mn_{0.40}Sn_{0.12}$ alloy films of three different thicknesses (14.5, 8.7, and 2.9 μm ± 0.5 μm) were synthesized by electrochemical deposition of a sequence of stacked elemental films on a tungsten substrate (W//$[Mn/Ni/Sn]_n$, n = 5, 3, 1), followed by a high temperature anneal (1273 K), resulting in a homogeneous, single-phase alloy

film (Fig. 1a). Detailed conditions of deposition and annealing were reported previously [5,19]. To isolate the role of the film/substrate interface, we produced free-standing grains and free-standing annealed films. 14.5 and 8.7 μm thick free-standing grains were obtained by ultrasonicating annealed films on substrates in deionized water (Fig. 1b). This process was sufficient to loosen and detach individual grains, which were filtered and then collected on thermally conductive copper tape. These grains have two clearly discernable faces, the free surface (smoother) and the delaminated surface (rougher; Fig. S1). 2.9 μm thick grains cannot be released using this method. Free-standing annealed films were produced by delaminating the deposited multi-layer films prior to annealing, and annealing suspended free-standing multi-layer films to obtain homogeneous single-phase alloy films (Fig. 1c). Cross-section images of 14.5 μm thick films showed approximately uniform film thickness (Fig. S2). Compositions, crystal structures, and exothermic (cooling) and endothermic (heating) peak transformation temperatures of alloy films were identified by energy dispersive spectroscopy, X-ray diffraction, and differential scanning calorimetry (DSC) (Fig. S3), respectively [5]. Optical observation of grain phase transformations was carried out on a BX53M Olympus polarized light microscope equipped with a differential interference contrast (DIC) prism. During observation, films and grains were heated and cooled at 1 K/min using a Linkam LTS 120 temperature controlled stage (– 25 to 120) ± 0.1 K. TA Q2000 was used for DSC tests, which were ramped at 10 K/min. Transmission electron microscopy (TEM) and scanning transmission microscopy (STEM) were used to further investigate the morphology and chemical composition of the films. Cross-sectional TEM lamellas from both free-standing and on-substrate films were prepared using a FEI Helios Nanolab 460F1 dual-focused ion beam (FIB). Bright-field imaging was then performed to study the microstructure on a FEI Tecnai G2 F20 Super-Twin FE-TEM operated at 200 kV. Film compositions have been verified by Scanning Electron Microscopy equipped with an Energy Dispersive Spectrometer (Fig. S4) [19].

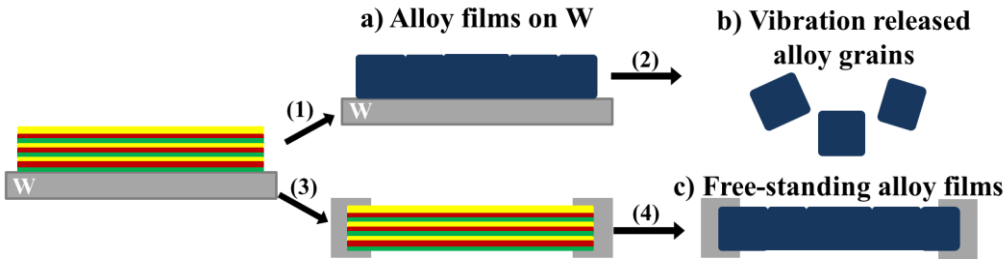

Fig. 1. Synthesis of a) alloy films on substrates, b) free-standing alloy grains, and c) free-standing alloy films following the steps: (1) anneal deposited multi-layer films, (2) release particles by mechanical vibration, (3) delaminate deposited multi-layer films, and (4) fix the edge of free-standing multi-layer films and anneal them.

Phase transformation progressions within individual grains in films on substrates, free-standing grains, and free-standing films, are consistent with thermoelastic

martensitic transformations, where continuous nucleation and growth of martensite domains occurs throughout the width of the transformation temperature to maintain local elastic and thermal equilibria [20,21]. Twenty-three grains (10 grains come from films on W, 7 grains come from free-standing films, and 6 grains come from free-standing grains) were selected randomly from the three sample geometries in order to compare their phase transformation progressions (TABLE SI, SII in supplementary material) [5]. 8.7 μm thick grains were used as examples to illustrate our observation (Fig. 2). We observed the change of the area fraction of each grain containing martensite during cooling and heating by using 7×7 grids/each 100 μm^2 to cover the image and calculate the percentage of grids with martensite plate in a grain. We found: 1) continuous nucleation and growth of martensite during cooling, 2) reversible disappearance of domains during heating, and 3) in most cases, the same positions of the disappearance of the last domain and the formation of the first domain. Martensite start temperature, M_s, (or austenite finish temperature, A_f) is defined as the temperature at which the first (or last) observed twin formed abruptly (or disappeared completely) on the surface during cooling (or heating) in a particular grain (Fig. 2). Although grains in these alloys show similar phase transformation progressions, the shape of the martensitic domains intersecting the free surface varies dramatically suggesting the orientation of martensite plates differ between different alloy forms. At the surface of both films on substrates and free-standing films, martensite plates appear to orient approximately perpendicular to the surface (Fig. S5a,c), whereas this preferred orientation is not as evident in free-standing grains (Fig. S5b). This similar phenomenon occurs in the same alloy forms with different thicknesses (Fig. S6).

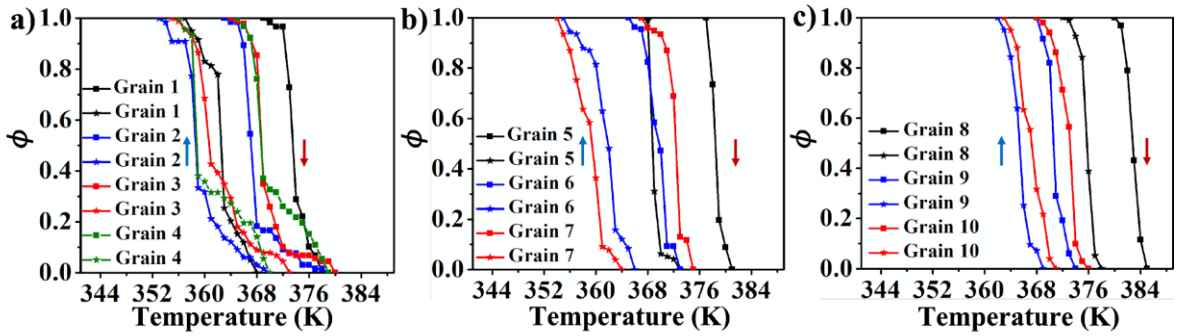

Fig. 2. Area fraction of a grain containing martensite during heating (line with square) and cooling (line with star) in 8.7 μm thick a) film on a substrate [5], b) free-standing grains, and c) free-standing film.

The thermal hysteresis (ΔT_{hyst} 0 = $A_f - M_s$), which is an accessible measure of hysteresis of each grain, is demonstrated to be a robust measure of the energy dissipated each cycle (E_{diss}) in the three alloy forms. When we assume that 1) irreversible dissipation is induced by frictional work, 2) the change of internal energy

of the universe (specimen plus surrounding) equals to zero, and 3) the heat capacity of austenite and martensite are same, E_{diss} could be calculated by multiplying the entropy change (ΔS) of $Ni_{0.48}Mn_{0.40}Sn_{0.12}$ alloys (~ 3.0 ± 0.3 J/(mol·K))[22] by the area inside the cycle [21]:

$$E_{diss} = \Delta S \cdot \oint \phi dT \qquad (1)$$

where ϕ represents the fraction of martensite inside a complete cycle. Using this equation, E_{diss} of randomly selected free-standing grains (TABLE SI) and grains in free-standing films (TABLE SII) are calculated and the corresponding thermal hysteresis of grains are listed. For films on substrates, E_{diss} = (2.80 ± 0.07)·ΔThyst 0J/mol, R^2 = 0.99 [5]. For free-standing grains, E_{diss} = (2.94 ± 0.10)·ΔThyst 0 J/mol, R^2 = 0.99, and for free-standing films, E_{diss} = (2.76 ± 0.04)·ΔThyst 0 J/mol, R^2 = 0.99 (Fig. 3a). E_{diss} is proportional to ΔThyst 0. Thus, we adopt ΔThyst 0 as an accessible measure of phase transformation hysteresis for individual grains.

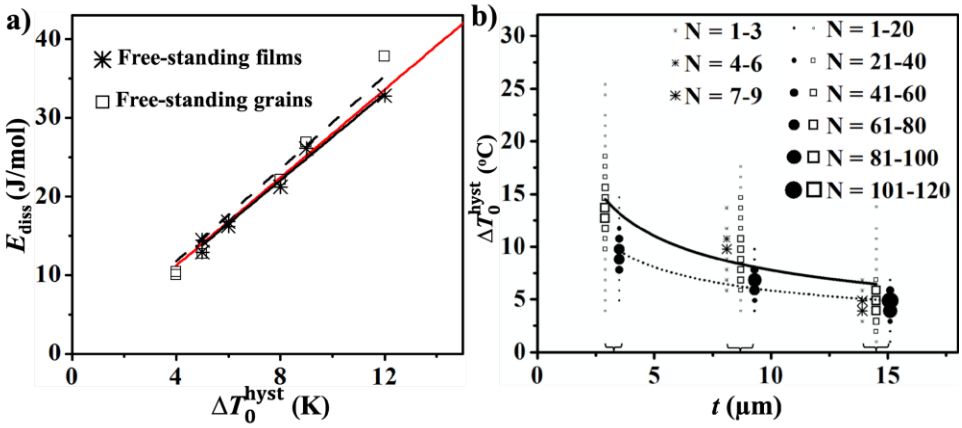

Fig. 3. a) Linear fits of E_{diss} on ΔThyst 0 of free-standing grains (dashed black line), free-standing films (solid black line), and films on substrates (red) [5], b) Power law fits of ΔThyst 0 on thickness of 14.5, 8.7, and 2.9 μm thick films on substrates (square) represented by a solid line [5], and free-standing films (circle) represented by a dot line. Asterisks represent the ΔThyst 0 of 14.5 and 8.7 μm thick free-standing grains. N represents the number of collected grains.

The distribution of collected A_f and M_s temperatures shows a different thickness-dependence of thermal hysteresis for different alloy forms. For the case of films on substrates, we have previously shown good agreement between the hysteresis determined by population statistics of grains and the hysteresis of an entire film determined by temperature-dependent XRD and DSC [5]. Linear correlations between A_f and M_s temperatures ($A_f = a_o + M_s$) of different alloy forms are observed and the hysteresis, a_o, is listed (Fig. S7, TABLE I) [5]. Hysteresis increases in thinner films in all cases. This phenomenon is consistent with previous conclusions that free surfaces and the film/substrate interfaces resist free motion of mobile domain boundaries [5,6].

However, it is clear that hysteresis is uniformly larger in the cases where the film was annealed while physically attached to the underlying substrate (films on substrates and free-standing grains).

TABLE I. a_o of linear fits between A_f and M_s temperatures of different alloy forms. The number of collected grains is shown in brackets.

Thickness	Film on substrate	Free-standing grains	Free-standing film
14.5 μm	4.84 ± 0.10 (382 grains)	4.64 ± 0.19 (20 grains)	4.45 ± 0.06 (300 grains)
8.7 μm	10.00 ± 0.13 (428 grains)	9.77 ± 0.38 (20 grains)	6.58 ± 0.07 (300 grains)
2.9 μm	14.22 ± 0.15 (470 grains)		9.52 ± 0.09 (300 grains)

Power law models are fit for comparing thickness-dependent hysteresis of the three alloy forms. In films on substrates, thickness-dependent hysteresis has been quantified by a power law model ($\Delta T_{hyst\,0} = a \cdot t^b$, a = 24.73, b = –0.50, 2.9 μm ⩽ t ⩽ 14.5 μm) [5]. In free-standing grains and films with a constant thickness, there are low correlations between $\Delta T_{hyst\,0}$ and area (S) or volume (V) (TABLE SIII) [23]. Besides, there are linear correlations between log S or log V and log t (thickness) (Fig. S8). Thus, the correlations between grain size and $\Delta T_{hyst\,0}$ are attributed to thickness, and the thickness-dependent hysteresis also is quantified by a power law model ($\Delta T_{hyst\,0} = a' \cdot t^{b'}$, a' = 15.07, b' = –0.42, 2.9 μm ⩽ t ⩽ 14.5 μm) in free-standing films (Fig. 3b). The models illustrate that removing substrates before annealing decreases hysteresis during martensitic transformations.

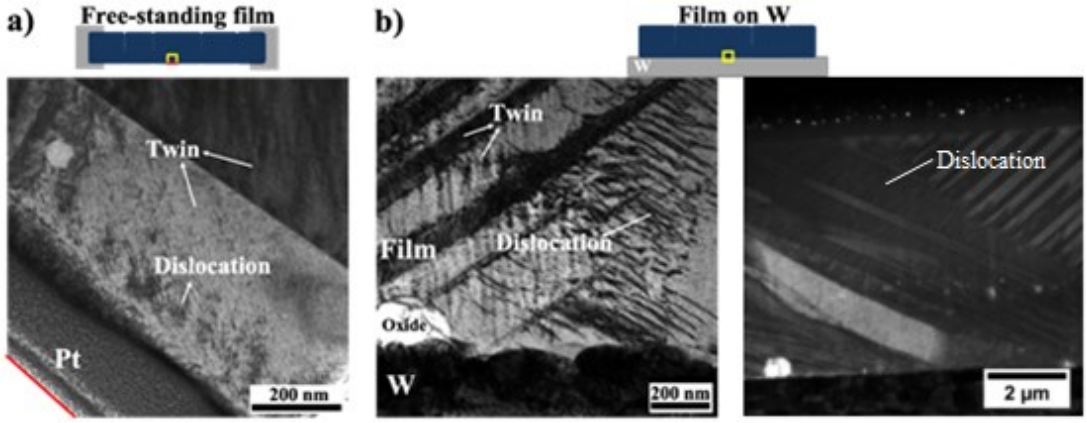

Fig. 4. Cross-sectional TEM micrographs of a) a 8.7 μm thick free-standing Ni-Mn-Sn film near the delaminated surface and b) a 8.7 μm thick Ni-Mn-Sn film on a W substrate showing the interface. The Mn-rich phase in b) was revealed by the high-angle annual dark-field imaging in STEM.

Cross-sections of a free-standing Ni-Mn-Sn film near the delaminated surface and the same film but on a W substrate were observed with TEM (Fig. 4). For the free-standing film, the free surface was protected by Pt layer to minimize FIB-beam damage. Fig. 4a illustrates a high density of short dislocation segments or loops with a weak contrast. They are consistent with Ga ion beam irradiation damage during FIB thinning. The observation suggests the martensite grains in the free-standing film do not contain many intrinsic crystallographic defects. For the Ni-Mn-Sn film attached on the substrate, Fig. 4b illustrates longer, well-defined dislocation lines which indicate a greater extent of localized plastic deformation. This observation is consistent with plastic deformation resulting from a mismatch in thermal expansion coefficients and cooling from an annealing temperature of 1273 K. Besides the dislocations, a secondary phase and a oxide phase were also noticed near the interface and might form during annealing (Fig. 4b). The secondary phase is free of twins, slightly Mn-rich, and only present in the film on W substrate. We do not anticipate the secondary phase undergoes phase transformation during thermal cycling. Additional chemical compositions could be found in Fig. S9 and S10.

We identify two key observations: 1) free surfaces serve to impede grain boundary motion (free-standing films) but not to the same degree as films supported on substrates, 2) removing substrates before annealing (free-standing films) decreases the hysteresis, while removing substrates after annealing (free-standing grains) does not significantly impact hysteresis. We infer that during cooling, the thermal expansion mismatch at the film/substrate interfaces increases residual stress in films, the concentration of dislocations at the interface, the secondary phase formed at the interface due to chemical diffusion, and the oxide phase near the interface, resulting in increased internal friction [17,24]. The observation of cross-sectional TEM micrographs is consistent with our inference that defects at the alloy/substrate interface work as a part of origins of thickness-dependent hysteresis (Fig. 3b).

In summary, we investigate the substrate effects by observing thermoelastic martensitic transformations of grains in films on W substrates, free-standing grains, and free-standing films. The thermal hysteresis increases with decreasing film thicknesses and is empirically fit with a power law model. After comparing the hysteresis of the three alloy forms and the cross-sectional TEM micrographs of their interface, we conclude that the thermal expansion mismatch at the film/substrate interfaces during the cooling process of heat treatment is primarily responsible for the reduced hysteresis from films on substrates to free-standing films with the same thickness.

Acknowledgements

This material is based upon work supported by the National Science Foundation under Grant No. 1636105.

Declarations of interest

The authors declare no competing interests.

Data availability statement

The datasets generated and analyzed during the current study are available from the corresponding author on reasonable request. All data generated or analyzed during this study are included in this published article and its supplementary information file.

References

[1] R. Zarnetta, R. Takahashi, M.L. Young, A. Savan, Y. Furuya, S. Thienhaus, B. Maaß, M. Rahim, J. Frenzel, H. Brunken, Identification of quaternary shape memory alloys with near-zero thermal hysteresis and unprecedented functional stability, Adv. Funct. Mater. 20 (2010) 1917-1923.
[2] E. Lovell, A.M. Pereira, A.D. Caplin, J. Lyubina, L.F. Cohen, Dynamics of the First-Order Metamagnetic Transition in Magnetocaloric La (Fe, Si) 13: Reducing Hysteresis, Adv. Energy Mater. 5 (2015) 1401639.
[3] S. Fähler, U.K. Rößler, O. Kastner, J. Eckert, G. Eggeler, H. Emmerich, P. Entel, S. Müller, E. Quandt, K. Albe, Caloric effects in ferroic materials: new concepts for cooling, Adv. Eng. Mater. 14 (2012) 10-19.
[4] R. Niemann, O. Heczko, L. Schultz, S. Fähler, Metamagnetic transitions and magnetocaloric effect in epitaxial Ni–Co–Mn–In films, Appl. Phys. Lett. 97 (2010) 222507.
[5] Y. Zhang, J. Billman, P.J. Shamberger, Size Effects in the Martensitic Transformation Hysteresis in Ni-Mn-Sn Heusler Alloy Films, Acta Mater. (2019).
[6] Y. Chen, C.A. Schuh, Size effects in shape memory alloy microwires, Acta Mater. 59 (2011) 537-553.
[7] T. Gottschall, D. Benke, M. Fries, A. Taubel, I.A. Radulov, K.P. Skokov, O. Gutfleisch, A Matter of Size and Stress: Understanding the First-Order Transition in Materials for Solid-State Refrigeration, Adv. Funct. Mater. 27 (2017) 1606735.
[8] F. Lambrecht, C. Lay, I.R. Aseguinolaza, V. Chernenko, M. Kohl, NiMnGa/Si shape memory bimorph nanoactuation, Shape Mem. Superelasticity 2 (2016) 347-359.
[9] S.M. Ueland, C.A. Schuh, Transition from many domain to single domain martensite morphology in small-scale shape memory alloys, Acta Mater. 61 (2013) 5618-5625.
[10] P. Ranzieri, S. Fabbrici, L. Nasi, L. Righi, F. Casoli, V.A. Chernenko, E. Villa, F. Albertini, Epitaxial Ni–Mn–Ga/MgO (1 0 0) thin films ranging in thickness from 10 to 100 nm, Acta Mater. 61 (2013) 263-272.
[11] J. Dong, J. Xie, J. Lu, C. Adelmann, C. Palmstrøm, J. Cui, Q. Pan, T. Shield, R. James, S. McKernan, Shape memory and ferromagnetic shape memory effects in single-crystal Ni 2 MnGa thin films, J. Appl. Phys. 95 (2004) 2593-2600.
[12] A. Diestel, P. Chekhonin, R. Niemann, W. Skrotzki, K. Nielsch, S. Fähler, Reducing Thermal Hysteresis in Epitaxial Ni–Mn–Ga–Co Films by Transformation Cycling, Phys. Status Solidi B 255 (2018) 1700330.
[13] R. Niemann, S. Hahn, A. Diestel, A. Backen, L. Schultz, K. Nielsch, M.-X. Wagner, S. Fähler, Reducing the nucleation barrier in magnetocaloric Heusler alloys by nanoindentation, Apl. Mater. 4 (2016) 064101.
[14] A. Diestel, R. Niemann, B. Schleicher, K. Nielsch, S. Fähler, Reducing Hysteresis Losses by Heating Minor Loops in Magnetocaloric Ni–Mn–Ga–Co Films, Energy Technol. 6 (2018) 1463-1469.
[15] N. Teichert, A. Auge, E. Yüzüak, I. Dincer, Y. Elerman, B. Krumme, H. Wende, O. Yildirim, K. Potzger, A. Hütten, Influence of film thickness and composition on the martensitic transformation in epitaxial Ni–Mn–Sn thin films, Acta Mater. 86 (2015) 279-285.

[16] A. Auge, N. Teichert, M. Meinert, G. Reiss, A. Hütten, E. Yüzüak, I. Dincer, Y. Elerman, I. Ennen, P. Schattschneider, Thickness dependence of the martensitic transformation, magnetism, and magnetoresistance in epitaxial Ni-Mn-Sn ultrathin films, Phys. Rev. B 85 (2012) 214118.
[17] M. Kuntz, B. Meier, G. Grathwohl, Residual stresses in fiber-reinforced ceramics due to thermal expansion mismatch, J. Am. Ceram. Soc. 76 (1993) 2607-2612.
[18] S. Doyle, V.A. Chernenko, S. Besseghini, A. Gambardella, M. Kohl, P. Müllner, M. Ohtsuka, Residual stress in Ni-Mn-Ga thin films deposited on different substrates, Eur. Phys. J. Spec. Top. 158 (2008) 99-105.
[19] Y. Zhang, P.J. Shamberger, Thick Film Ni 0.5 Mn 0.5− x Sn x Heusler Alloys by Multi−layer Electrochemical Deposition, Sci. Rep. 8 (2018) 11931.
[20] A. Cherechukin, I. Dikshtein, D. Ermakov, A. Glebov, V. Koledov, D. Kosolapov, V. Shavrov, A. Tulaikova, E. Krasnoperov, T. Takagi, Shape memory effect due to magnetic field-induced thermoelastic martensitic transformation in polycrystalline Ni–Mn–Fe–Ga alloy, Phys. Lett. A 291 (2001) 175-183.
[21] J. Ortin, A. Planes, Thermodynamic analysis of thermal measurements in thermoelastic martensitic transformations, Acta Metall. 36 (1988) 1873-1889.
[22] X. Moya, L. Mañosa, A. Planes, T. Krenke, M. Acet, E.F. Wassermann, Martensitic transition and magnetic properties in Ni–Mn–X alloys, Mater. Sci. Eng. A 438 (2006) 911-915.
[23] M.M. Mukaka, A guide to appropriate use of correlation coefficient in medical research, Malawi Med. J. 24 (2012) 69-71.
[24] L.B. Freund, S. Suresh, Thin film materials: stress, defect formation and surface evolution, Cambridge University Press, New York, 2004.

Substrate Effects in Hysteresis of Microscale Ni-Mn-Sn Heusler Alloy Films: Supplementary Info

Yijia Zhang[1]
Dexin Zhao[1]
Carlos Lago[1]
Kelvin Xie[1]
Patrick J. Shamberger[1]

[1] Department of Materials Science and Engineering
Texas A&M University
College Station, TX, 77843, USA

Phone: 979-458-1086
Fax: 979-862-6835
E-mail: patrick.shamberger@tamu.edu

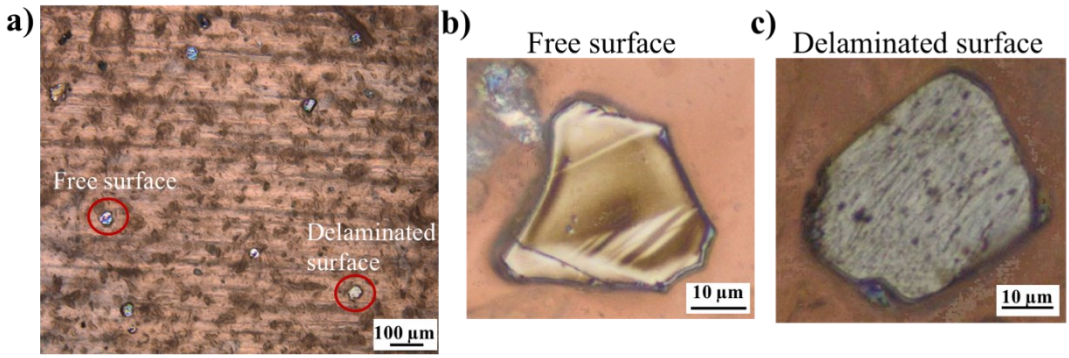

Fig. S1. a) 14.5 µm thick free-standing alloy grains on the thermal conductive copper tape, b) free surface and c) delaminated surface of 14.5 µm thick free-standing alloy grains.

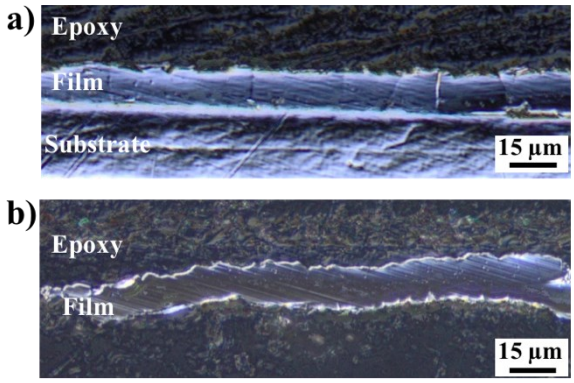

Fig. S2. The cross-section images of 14.5 µm thick a) alloy film on a tungsten substrate and b) free-standing annealed alloy film using differential image contrast.

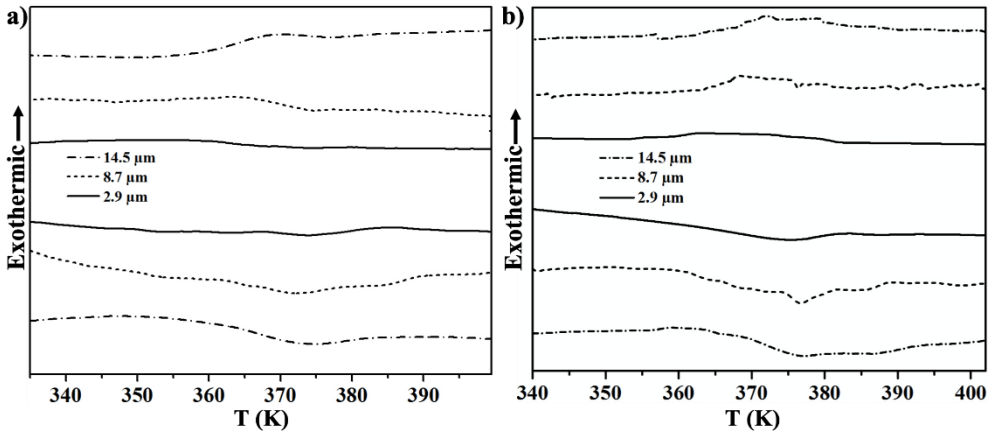

Fig. S3. The DSC measurements of a) alloy films on W substrates and b) free-standing annealed alloy films.

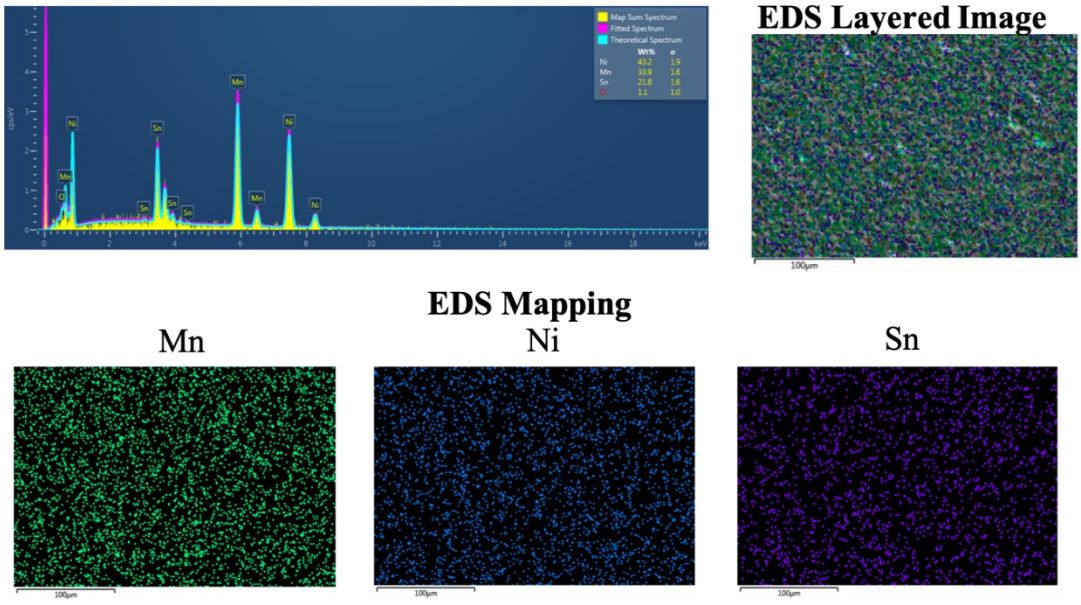

Fig. S4. Composition analysis of 8.9 µm thick alloy films by EDS. Peak at 0 keV is caused by electronic noise.

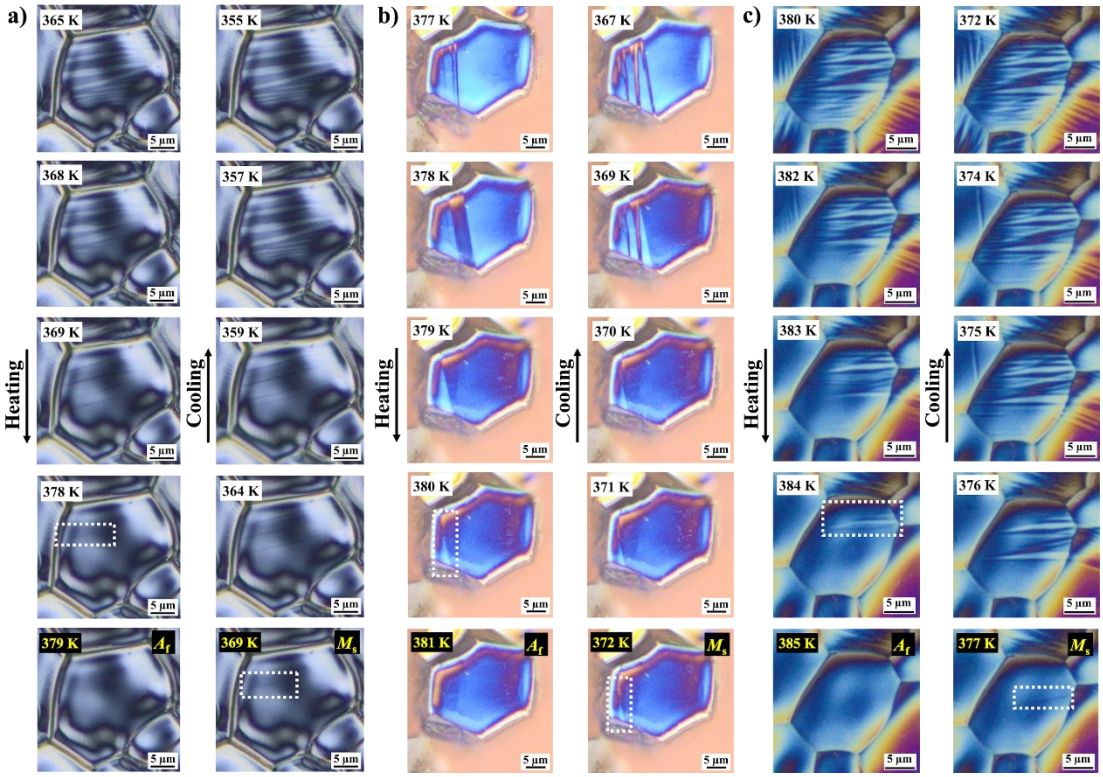

Fig. S5. Disappearance and formation of martensitic domains in 8.7 µm thick a) grain 4, b) grain 5, and c) grain 8 during heating and cooling observed by DIC.

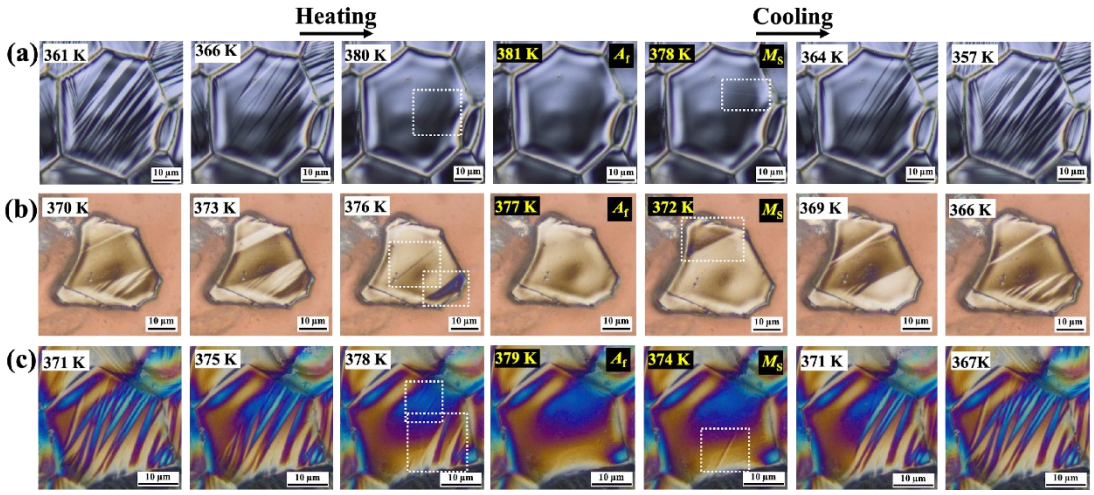

Fig. S6. Disappearance and formation of martensitic domains (observed by DIC) in a) one grain from 14.5 µm thick alloy film on W, b) a 14.5 µm thick free-standing grain, and c) one grain from the 14.5 µm thick free-standing film during heating and cooling.

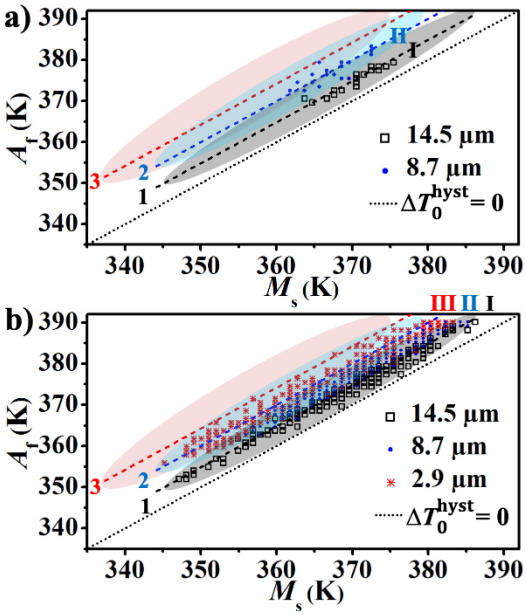

Fig. S7. Linear fits of A_f on M_s temperatures of a) 14.5 (I, black solid line) and 8.7 (II, blue solid line) µm thick free-standing grains, and b) grains in 14.5 (I, black solid line), 8.7 (II, blue solid line), and 2.9 (III, red solid line) µm thick free-standing films. Gray, blue, and red contour show the distributions of collected grains in 14.5, 8.7, and 2.9 µm thick films on substrates, respectively. Black (1), blue (2), and red (3) dashed lines show the linear fits of the A_f on M_s temperatures of 14.5, 8.7, and 2.9 µm thick films on substrates, respectively.

TABLE SI. Area, phase transformation temperatures, and thermal hysteresis in select grains from free-standing alloy grains.

Grain	5	6	7	11	12	13
Grain area, S (µm^2)	536	172	319	682	667	899
Thickness, t (µm)	8.7	8.7	8.7	14.5	14.5	14.5
$\underline{D}^a/t$	3.0	1.7	2.3	2.0	2.0	2.3
A_f (K)	381	373	375	374	377	377
M_s (K)	372	365	363	370	372	373
ΔThyst 0(K)	9	8	12	4	5	4
E_{diss} (J/mol^b)	26.9	22.1	37.8	10.4	12.7	10.0

[a] $\underline{D} = \sqrt{4S/\pi}$
[b] Per mole of atoms

TABLE SII. Area, phase transformation temperatures, and thermal hysteresis in select grains from free-standing alloy films.

Grain	8	9	10	14	15	16	17
Grain area, S (µm^2)	224	232	313	192	60	1899	734
Thickness, t (µm)	8.7	8.7	8.7	2.9	2.9	14.5	14.5
$\underline{D}^a/t$	1.9	2.0	2.3	5.4	3.0	3.4	2.1
A_f (K)	385	374	376	361	370	371	379
M_s (K)	377	368	370	352	358	366	374
ΔThyst 0(K)	8	6	6	9	12	5	5
E_{diss} (J/mol^b)	21.2	16.2	16.8	26.1	32.8	14.4	12.9

[a] $\underline{D} = \sqrt{4S/\pi}$
[b] Per mole of atoms

TABLE SIII. Pearson's correlation coefficient, r, between grain ΔThyst 0 and S or V of free-standing grains and films (we only consider the absolute value of r).

r	ΔThyst 0 and S or V
14.5 µm thick grains	0.24
8.7 µm thick grains	0.06
14.5 µm thick film	0.07
8.7 µm thick film	0.12
2.9 µm thick film	0.02

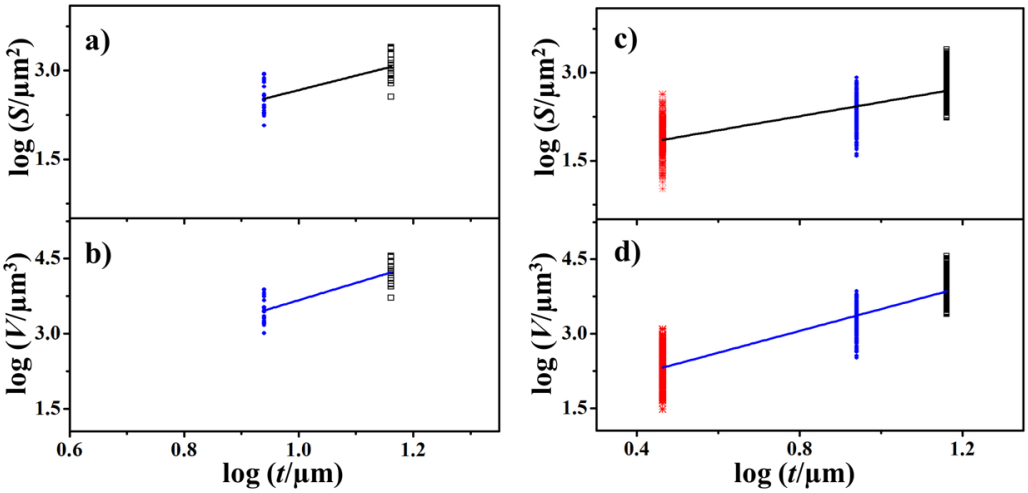

Fig. S8. Linear fits of a) log S on log t and b) log V on log t in 14.5 (black square) and 8.7 (blue circle) µm thick free-standing alloy grains, and c) log S on log t and d) log V on log t in 14.5 (black square), 8.7 (blue circle), and 2.9 (red asterisk) µm thick free-standing alloy films.

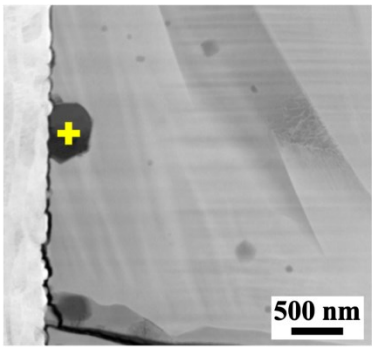

Fig. S9. Composition of the oxide at the film/W interface acquired by point EDS. Cu from the TEM sample holder.